Accepted Manuscript

Submission Date: 2023-12-31
Accepted Date: 2024-03-14
Accepted Manuscript online: 2024-03-20

Organic Materials

Diazananographene with Quadruple [5]Helicene Units: Synthesis, Optical Properties, and Supramolecular Assembly

Xiao-Hui Ma, Jiang-Feng Xing, Ling Chai, Qing-Song Deng, Xuan-Wen Chen, Hai-Feng Su, Chao Li, Yuan-Zhi Tan.

Affiliations below.

DOI: 10.1055/a-2291-8673

Please cite this article as: Ma X-H, Xing J-F, Chai L et al. Diazananographene with Quadruple [5]Helicene Units: Synthesis, Optical Properties, and Supramolecular Assembly. Organic Materials 2024. doi: 10.1055/a-2291-8673

Conflict of Interest: The authors declare that they have no conflict of interest.

This study was supported by National Natural Science Foundation of China (http://dx.doi.org/10.13039/501100001809), 92061103, 21721001, 22101241

Abstract:
A helical diazananographene (1) was synthesized using sterically hindered t-butyl groups to inhibit further dehydrocyclization of [5]helicene units. These t-butyl groups stabilized the conformation of [5]helicene units, thus resulting in three stable conformers of 1, comprising a pair of enantiomers (1-(P, P, P, P) and 1-(M, M, M, M)) and a mesomer (1-(P, P, M, M)). In comparison to its planar analogs, helical 1 exhibited broadened peaks in its absorption and emission spectra, with an increase in the emission quantum yield from 0.3 to 0.6. The significantly enhanced radiative decay rate (kr) accounted for the increase in the quantum yield of 1. It was found that 1 could be fully protonated upon the addition of an equivalent acid. Furthermore, 1 assembled into a chiral trimeric metallosupramolecular complex upon coordination with the PdII units. Both protonated 1 and the metallosupramolecular complex of 1 exhibited an enhanced circular dichroic response. These findings revealed that the incorporation of a helical structure and pyridinic nitrogen-doping into the nanographene can allow the synthesis of responsive chiroptical graphenic materials, which can serve as building blocks for chiral hierarchical metallosupramolecular structures.

Corresponding Author:
Prof. Yuan-Zhi Tan, Xiamen University, chemistry, simin nan road 422-18, 361005 xiamen, Germany, yuanzhi_tan@xmu.edu.cn

Affiliations:
Xiao-Hui Ma, Xiamen University, chemistry, xiamen, China
Jiang-Feng Xing, Xiamen University, chemistry, xiamen, China
Ling Chai, Xiamen University, chemistry, xiamen, China
[...]
Yuan-Zhi Tan, Xiamen University, chemistry, xiamen, Germany

Diazananographene with Quadruple [5]Helicene Units: Synthesis, Optical Properties, and Supramolecular Assembly

Xiao-Hui Ma[a], Jiang-Feng Xing[a], Ling Chai[a], Qing-Song Deng[a], Xuan-Wen Chen[a], Hai-Feng Su[a], Chao Li[b,c] *, Yuan-Zhi Tan[a]*

[a] State Key Laboratory for Physical Chemistry of Solid Surfaces, Department of Chemistry, College of Chemistry and Chemical Engineering, Xiamen University, Xiamen, 361005, China

[b] SINOPEC Maoming Company，Maoming 525000, China

[c] Beijing University of Chemical Technology, Beijing, 100000, China

*Correspondence to: yuanzhi_tan@xmu.edu.cn; lich5449.mmsh@sinopec.com

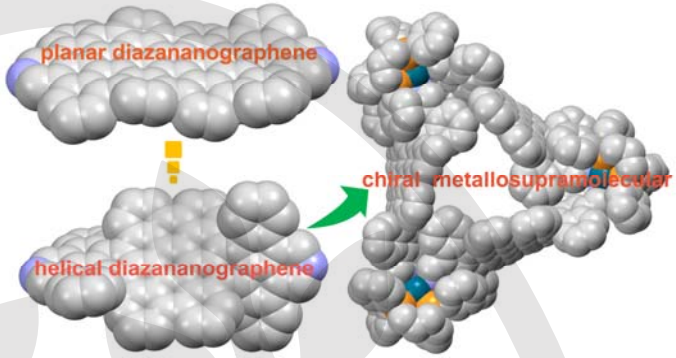

Received:
Accepted:
Published online:
DOI:

Abstract A helical diazananographene (**1**) was successfully synthesized by employing sterically hindered *t*-butyl groups to inhibit further dehydrocyclization of [5]helicene units. These *t*-butyl groups stabilized the conformation of [5]helicene units, thus resulting in three stable conformers of **1**, comprising a pair of enantiomers (**1**-(*P*, *P*, *P*, *P*) and **1**-(*M*, *M*, *M*, *M*)) and a mesomer (**1**-(*P*, *P*, *M*, *M*)). In comparison to its planar analogs, helical **1** exhibited broadened peaks in both its absorption and emission spectra, leading to an increase in the emission quantum yield from 0.3 to 0.6. The significantly enhanced radiative decay rate (k_r) accounted for the increase in the quantum yield of **1**. Additionally, it was observed that the compound could be fully protonated upon the addition of an equivalent acid. Furthermore, **1** assembled into a chiral trimeric metallosupramolecular complex upon coordination with the Pd^{II} units. Both protonated **1** and the metallosupramolecular complex exhibited an enhanced circular dichroic response. These findings revealed that the incorporation of a helical structure and pyridinic nitrogen-doping into the nanographene can allow the synthesis of responsive chiroptical graphenic materials, which could serve as fundamental components for constructing chiral hierarchical metallosupramolecular structures.

Key words diazananographene; [5]helicene; optical properties; supramolecular assembly

Introduction

The physical and electronic characteristics of nanographene can be altered by adjusting its size[1,2], its edge structures[3-5], and through doping of heteroatoms[6-8]. These parameters can thus be used for fine-tuning various material properties such as energy gap, optical features, and the redox behavior of nanographene[9-11]. Among the heteroatom doping, pyridinic nitrogen doping has attracted considerable attention owing to its dual impact, as it not only allows fine-tuning of the above-mentioned electronic and optical properties of nanographene but also facilitates the formation of nanographene-based metallosupramolecular complexes by providing sites for coordination with metals[12-14]. Till now, most pyridinic nitrogen-doped nanographene-based materials exhibit a planar structure[15,16] that do not exhibit chirality.

The incorporation of helical structures into planar nanographene can induce asymmetry, resulting in stereoisomerism and chiroptical properties[17-21]. The pyridinic nitrogen atoms located at the skeleton of nanographene can be protonated or can coordinate with protons or metal ions, owing to their lone electron pairs[22-24]. Consequently, the coexistence of pyridinic nitrogen-doped atoms and helical structures within a molecule enables the modulation of their intrinsic electronic and optical properties and facilitates the manipulation of their chiroptical characteristics through mechanisms such as metal coordination or protonation[25,26]. In recent years, numerous helicenes with pyridinic nitrogen doping have been synthesized and employed as chiral switches[27-30]. This demonstrates that the chiroptical properties of nitrogen-doped helicenes can be tailored through coordination, protonation, or other reactions involving pyridinic nitrogen[31-33]. Based on these results, it was hypothesized that the simultaneous incorporation of helical chirality and pyridinic nitrogen doping could then be employed to yield chiral nitrogen-doped nanographene. This study can therefore serve as an illustrative example for exploring how properties of nanographene may be regulated and tuned *via* chirality and pyridinic nitrogen doping. However, synthesis of such kind of nanographene molecules has so far not been reported in literature.

In this work, a diazananographene sample with quadruple [5]helicene units was synthesized by incorporating sterically hindered *t*-butyl groups to inhibit further dehydrocyclization of the [5]helicene units during the Scholl reaction. Owing to the hindrance offered by the *t*-butyl groups at the [5]helicene unit, **1** exhibited three stable conformers, namely **1**-(*P*, *P*, *P*, *P*), **1**-(*P*, *P*, *M*, *M*) and **1**-(*M*, *M*, *M*, *M*), which were separated by high-performance liquid chromatography (HPLC). The conformer structures of **1** subsequently determined through single-crystal

X-ray diffraction (XRD). In comparison to its analogous planar diazananographene (**2**), the helical **1** structure exhibited broader peaks in its absorption and fluorescence spectra, along with increased fluorescence quantum yield and reduced fluorescence lifetimes. The conformers **1**-(*P*, *P*, *P*, *P*) and **1**-(*M*, *M*, *M*, *M*) exist as a pair of enantiomers that exhibited circular dichroic (CD) responses extending up to an optical wavelength of 560 nm. A racemization barrier value of 32.1 kcal mol^{-1} was obtained using computational methods, whereas its experimental value was found to be 29.6 kcal mol^{-1} by the HPLC-based thermal isomerization results. The protonation of **1**-(*P*, *P*, *P*, *P*) was then investigated, which revealed an equivalent bonding capacity to protons. After protonation, its CD response redshifted from 560 nm to 605 nm. Furthermore, the structure of **1**-(*P*, *P*, *P*, *P*) also displayed the ability to assemble with (*cis*-dppp)Pd^{II} units, thereby forming the triangular metallosupramolecular trimer (**3**) with enhanced chiroptical response compared to the monomeric conformer of **1**.

Results and Discussion

In Figure 1, the synthesis of diazananographenes **1** and **2** was depicted. Compound **8** was prepared *via* the iridium-catalyzed borylation reaction of tetra-*t*-butyl hexa-peri-hexabenzocoronene (HBC). Thereafter, compound **8** was coupled with **7** through the Suzuki–Miyaura coupling reaction to obtain precursor **6**. Then, cyclodehydrogenation of **6** with $FeCl_3$ and CH_3NO_2 was carried out to prepare the reddish-orange planar nanographene structure **2** with a yield of 57%. The planar nanographene structure **2** was characterized by ^1H NMR spectroscopy and high-resolution matrix-assisted laser desorption-ionization time-of-flight mass spectrometry (MALDI-TOF MS) (refer to inset in Figure 1). The observed m/z value and isotopic pattern were in agreement with the simulated results (calculated for $\mathbf{C_{108}H_{88}N_2}$, 1413.668; found, 1413.665). The planar structure of compound **2** was further determined using single-crystal XRD. The carbon skeleton of **2** was slightly twisted owing to the peripheral bulky groups (Figure S6). For the synthesis of helical diazananographene **1**, precursor **4** was obtained by replacing compound **7** with compound **5** following a similar synthetic pathway as that used for precursor **6**. Subsequently, the dehydrocyclization of **4** was carried out using 2,3-dichloro-5,6-dicyano-1,4-benzoquinone (DDQ) in dichloromethane (DCM)/triflic acid (TfOH) at a temperature of 0 °C, to resulting in the formation of the orange-yellow solid **1**. The resulting produced **1** was characterized by mass spectrometry and NMR analyses (see Figure 1).

For further verification of the helical structure of **1**, single crystals were cultivated by the gradual evaporation of CH_3OH into a solution of 1,1,2,2-tetrachloroethane containing all three fractions that were obtained from HPLC (Figure S10). The data obtained for the prepared crystals clearly showed that the configuration of the first chiral HPLC fraction of compound **1** belonged to the conformer **1**-(*P*, *P*, *P*, *P*), as depicted in Figure 2a. The circular dichroism (CD) spectra obtained were consistent with these findings, providing additional support for the results. Single-crystal X-ray diffraction (SCXRD) analysis further revealed a homochiral crystal structure of **1**-(*P*, *P*, *P*, *P*), with a cruciform-shaped quadruple helical skeleton. The dihedral angles ranged from 32.45° to 36.44° in the helical structures (see Figure 2a), with an average angular value of 34.78°. The range of dihedral angles for **1**-(*P*, *P*, *P*, *P*) was significantly different in comparison to the previously reported [5]helicenes[34]. The significant variation in bond lengths was observed in the fjord region within the [5]helicene subunit, which ranged from 1.41 Å to 1.46 Å, as shown in Figure 2c. The crystal structure belonged to the $P2_12_12_1$ space group, with four homochiral structures present in each unit cell, which formed a herringbone packing through the C-H···π interactions (Figure S11).

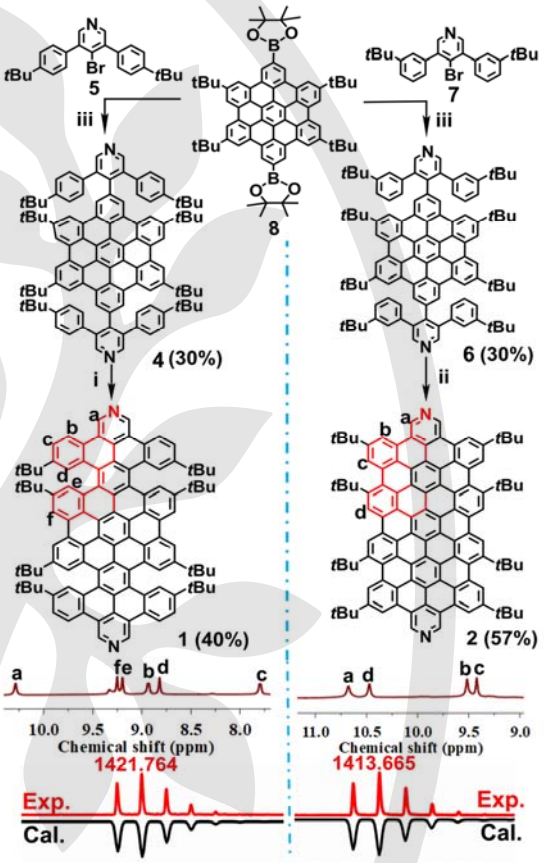

Figure 1. Synthesis of **1** and **2**. (i) DDQ, TfOH, dichloromethane (DCM), 0 °C, 1.0 h; (ii)$FeCl_3$, CH_3NO_2, DCM, 25 °C, 1.0 h; (iii) $Pd(PPh_3)_4$, Cs_2CO_3, 1,4-dioxane/H_2O = 4/1, v/v, 105 °C, 24 h. The mass and ^1H NMR spectra are provided in the insets.

The crystal structure obtained from the second chiral HPLC fraction consisted of the four helicene parts, resulting in a meso-type achiral conformer **1**-(*P*, *P*, *M*, *M*), as shown in Figure 2b. The dihedral angle was measured at approximately 34.0°, and the inner helical bond lengths ranged from 1.40 Å to 1.46 Å (Figure 2d). The unit cell of **1**-(*P*, *P*, *M*, *M*) contained two crystallographically independent molecules, and adjacent molecules were shaped into one-dimensional columnar stacking structures *via* the C-H···π interactions (Figure S12). The CD spectra of the first and third peaks displayed opposite Cotton effects (Figure 4a), indicative of the presence of helical enantiomers.

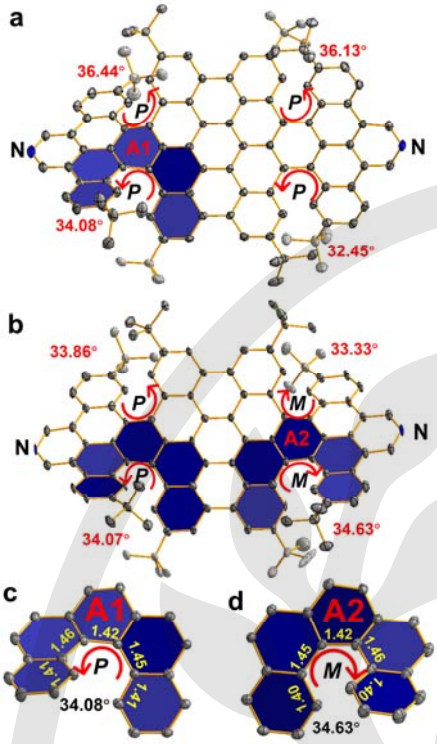

Figure 2. (a-b) Crystal structure and torsion angles of **1**-(*P*, *P*, *P*, *P*) and **1**-(*P*, *P*, *M*, *M*). The structure is depicted using the ORTEP model with thermal ellipsoids drawn at a 50% probability level. (c-d) Bond lengths of the inner helix in the **1**-(*P*, *P*, *P*, *P*) and **1**-(*P*, *P*, *M*, *M*) structures.

The optical properties of the planar nanographene (**2**) and the helical nanographene (**1**) were analyzed and compared through UV/Vis absorption and emission spectroscopies (Figure 3). The primary absorption peaks observed for **1** and **2** were detected at wavelengths of 430 nm and 446 nm, respectively. The absorption spectrum of **1** displayed a blue shift of 16 nm in comparison to **2**, along with a notable decrease in the molar extinction coefficient value, attributed to the more flexible helical structures. The optical HOMO-LUMO gap of **1** was calculated to be 2.21 eV, which exceeded the corresponding value for **2** (2.13 eV). Additionally, Density functional theory (DFT) calculations were performed as well (Figure S13). The calculated energy gap between HOMO and LUMO of **1** was found to be 2.65 eV, contrasting with the energy gap of 2.49 eV for planar nanographene (**2**), aligning with the experimental findings.

Additionally, apart from slight bathochromic shifts in the fluorescence spectrum of **1**, in comparison to the spectrum obtained for **2**, a clear broadening of the peaks for **1** was also seen in Figure 3a. The fluorescence quantum yield of **1** reached up to 60%, which was approximately double the value obtained for compound **2** (30%). The photoluminescence (PL) dynamics of both compounds were examined through time-resolved PL spectroscopy. The obtained time-resolved fluorescence decays for compounds **1** and **2** were fitted using monoexponential functions, revealing fluorescence lifetimes of τ_1 = 7.0 ns and τ_2 = 23.3 ns for compounds **1** and **2**, respectively. Additionally, the radiative (k_r) and nonradiative decay (k_{nr}) rate constants were also calculated (k_r = 8.56 × 10^7 s^{-1} for **1** and 1.29 × 10^7 s^{-1} for **2**, k_{nr} = 5.71 × 10^7 s^{-1} for **1** and 3.01 × 10^7 s^{-1} for **2**) based on their respective PL lifetimes and quantum yields. The results suggested that the significantly enhanced value of k_r may be responsible for the increase in the PL signal in **1**.

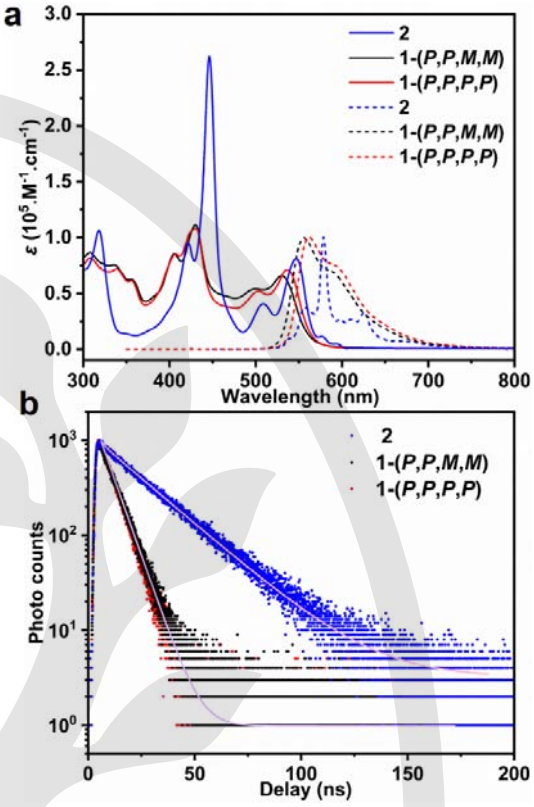

Figure 3. (a) The obtained UV/Vis (solid line) and fluorescence spectra (broken line) for **1**-(*P*, *P*, *P*, *P*), **1**-(*P*, *P*, *M*, *M*) and **2**. (b) Fluorescence decay curves for **1**-(*P*, *P*, *P*, *P*), **1**-(*P*, *P*, *M*, *M*) and **2** obtained from time-resolved PL spectroscopy.

The electrochemical behaviors of **1** and **2** were then investigated using cyclic voltammetric (CV) analyses in DCM (Figure S14). Only one reversible oxidation wave with a half-wave potential of $E^{ox}_{1/2}$= 0.95 V (*vs* Fc^+/Fc; Fc: ferrocene) was observed in **1**. Conversely, compound **2** displayed one irreversible and one reversible oxidation wave, with the latter having a half-wave potential of $E^{ox}_{1/2}$= 0.82 V. Electrochemical oxidation is generally linked to the energy level of the highest occupied molecular orbital (HOMO). The HOMO energy level for **1** was computed to be approximately −4.90 eV, which was 0.13 eV lower than that found for **2** (−4.77 eV) (Figure S13). This was also consistent with the experimental CV measurements that were obtained.

The two helical enantiomers of **1** were successfully separated using HPLC on a Daicel Chiralpak IE column employing an eluent composed of isopropyl alcohol and dichloromethane in a 1:19 ratio. Subsequent characterization was carried out using circular dichroism (CD) spectroscopy. The two isolated enantiomers were found to be perfect mirror images of each other, as shown in Figure 4. This resulted in a pronounced Cotton effect within the 320−400 nm wavelength range, with a corresponding $|\Delta\varepsilon|$ value of 227 M^{-1} cm^{-1} at a wavelength of 357 nm. The simulated CD spectra, generated through TD-DFT calculations at the PBE0-D3(BJ)/6-311G(d) level[35-38], closely matched the experimental findings. This validation confirmed that the first and third fractions corresponded to the isomers **1**-(*P*, *P*, *P*, *P*) and **1**-(*M*, *M*, *M*, *M*), respectively, consistent with SCXRD analysis.

One of the key stereo-dynamic characteristics of helicenes and their related compounds is their configurational stability, which can be assessed by the Gibbs activation energy ($\Delta G^{\neq}(T)$) of enantiomerization. In this study, the conformational stability of **1** was investigated through DFT calculations at the B3LYP-D3(BJ)/6-31G(d) level. The most stable isomer was **1**-(*P*, *P*, *M*, *M*) with a relative Gibbs free energy of -1.2 kcal mol^{-1}. Comparatively, the Gibbs free energy of **1**-(*P*, *P*, *P*, *M*) was 6.1 kcal mol^{-1} higher than that of **1**-(*P*, *P*, *P*, *P*). The helicity inversion from**1**-(*P*, *P*, *P*, *P*) to **1**-(*P*, *P*, *P*, *M*) involved a transition through the TS1 transition state with an energy barrier of 32.1 kcal mol^{-1}, corresponding to rate constants of 1.8×10^{-11} s^{-1} at 25 ℃ and 3.8×10^{-6} s^{-1} at 120 ℃. This indicates that achieving a conformational change in **1** at room temperature is challenging but feasible at higher temperatures such as 120 ℃. The intermediate **1**-(*P*, *P*, *P*, *M*) crossed through the transition state TS2 having an energy barrier of 26.1 kcal mol^{-1} to form **1**-(*P*, *P*, *M*, *M*). Furthermore, the interconversion process from **1**-(*P*, *P*, *P*, *P*) to **1**-(*P*, *P*, *M*, *M*) was further evaluated using chiral HPLC under heating (Figure S15). The half-life ($\tau_{1/2}$) for the loss in enantiomeric excess was determined to be 68 min. It provided a racemization barrier $\Delta G^{\neq}$ of 29.6 kcal mol^{-1} (at 393 K) calculated using the Eyring equation. These findings highlight the relatively stable nature of helicene enantiomer in comparison to previously reported [5]helicene-based nanographene molecules[39-40].

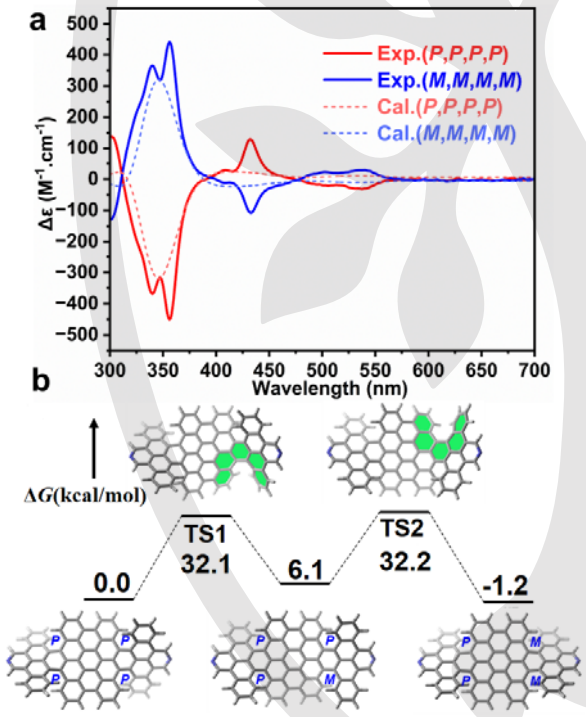

Figure 4. (a) The obtained CD spectra of **1**-(*P*, *P*, *P*, *P*) and **1**-(*M*, *M*, *M*, *M*) in dichloromethane (10^{-5} M, 298 K). The dotted line shows the simulated CD spectrum of **1**-(*P*, *P*, *P*, *P*) and **1**-(*M*, *M*, *M*, *M*) obtained by TD-DFT calculations at the PBE0-D3(BJ)/6-311G(d) level. (b) Energy profile for the isomerization of **1** at the B3LYP-D3(BJ)/6-31G(d) level of DFT.

The nitrogen atoms on the backbone of the nanographene structure can easily be protonated and deprotonated owing to the unpaired electrons, which leads to significant changes in its optical properties upon exposure to acidic solutions. The sensitivity of **1** to acids was evaluated through an examination of changes observed in the UV-Vis and fluorescence spectra upon the introduction of trifluoroacetic acid (TFA). During the addition of up to 2.0 molar equiv. of TFA to the DCM solution of **1**, a reduction in the intensity of the absorption peak at 430 nm was observed, accompanied by the emergence of a new broad absorption peak at 450 nm in the spectrum (Figure 5a). Further addition of TFA up to 5.0 molar equiv. did not substantially affect the absorption spectrum, indicating that the formation of **1**+2H$^+$ was almost saturated after the addition of 2.0 molar equiv. of TFA. Notably, the complete recovery of the protonated structure **1** was achieved by introducing an equivalent concentration of triethylamine (TEA), demonstrating the reversible nature of its protonation in the solution.

The CD spectra of chiral conformers of **1** were also modified significantly upon protonation by TFA. The addition of 5 molar equivalents of TFA to **1**-(*P*, *P*, *P*, *P*) in DCM resulted in the emergence of new CD peaks within the wavelength ranges of 300–438 nm, 438–500 nm, and 565–605 nm. A pronounced Cotton effect was observed at wavelengths beyond 438 nm. Although the intensity of the CD signals ($\Delta\varepsilon$) exhibited a slight reduction in the wavelength range of 300–438 nm, the peak wavelength was red-shifted from 555 nm to 605 nm. This implied that protonation by TFA led to enhanced absorbance in the low-energy transition region.

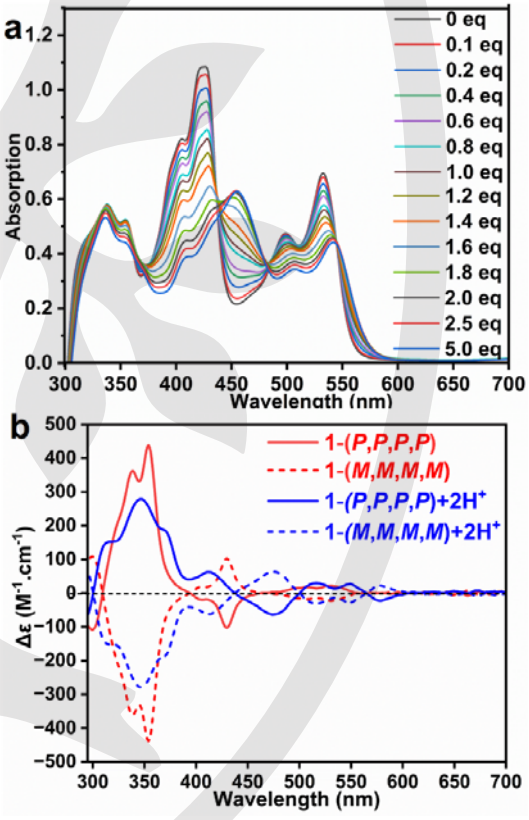

Figure 5. (a) Changes in the UV–Vis absorption spectra upon titration of **1**-(*P*, *P*, *P*, *P*) (2×10^{-5} M in DCM) with TFA. (b) The obtained CD spectra of **1** (red) and **1**+2H$^+$ (blue) in DCM.

The chiral metallaprisms (**3**) were constructed through the coordination-driven self-assembly of **1**-(*P*, *P*, *P*, *P*) and Pd(dppp)(OTf)$_2$ in DCM. Analysis of the 1H NMR spectrum of the resulting complex revealed distinct signals compared to those observed in the spectrum of **1**-(*P*, *P*, *P*, *P*), as shown in Figure 6b. The high-resolution electronic spray ionization (ESI) mass spectrometry provided the precise molecular formula for this complex. The predominant signals in the ESI spectrum were

centered around m/z = 3659.60 (z = 2) with signals spaced by 0.500 mass units, as illustrated in Figure 6c. These signals can be assigned to the metallosupramolecular trimer (**3**) after it has lost two triflate anions. The structure of **3** was optimized using DFT calculations at the PBE0-D3/3-21G level. The results of these calculations showed that **3** exhibited a triangular prism-shaped structure composed of nanographene walls with Pd^{II} ions situated at the vertices (Figure 6a). A lower red-shift of 25 nm was observed in the absorption spectrum of **3** in comparison to **1**-(*P*, *P*, *P*, *P*). The PL spectrum of **3** displayed a similar profile to that of the **1**-(*P*, *P*, *P*, *P*) conformer, although the strongest peak was red-shifted to 583 nm, as shown in Figure 6d. The red-shifted absorption and emission peaks with similar spectral shapes may be attributed to the bonding interaction between **1**-(*P*, *P*, *P*, *P*) and the Pd^{II} ions at the corners. Meanwhile, the formation of **3** not only caused red-shifts in the CD spectra (Figure 6e) but also led to an enhancement in the CD response.

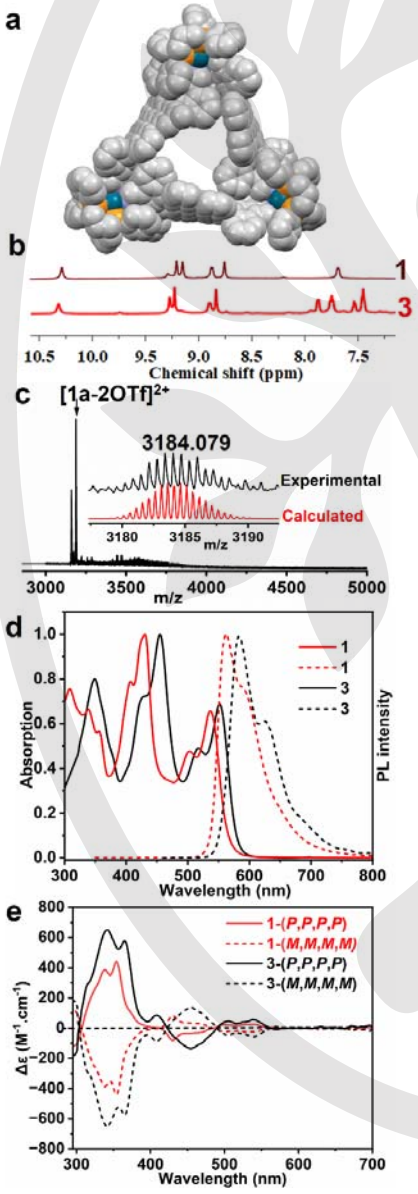

Figure 6. (a) Optimized structure of **3** obtained from DFT calculations. (b) The obtained ^{1}H NMR spectra for **1** and **3**. (c) The obtained ESI-MS spectra for **3**. The inset shows the isotopic distribution, which is in agreement with the calculated pattern. (d) Absorption (solid lines) and emission (dashed lines) spectra for **1** (red) and **3** (black) in DCM. (e) The obtained CD spectra for **1** (red) and **3** (black) in DCM.

Conclusions

In summary, a diazananographene containing quadruple [5]helicene units (**1**) and its planar counterpart (**2**) were successfully synthesized. The [5]helicene units were formed from the adjacent *t*-butyl groups positioned in opposite directions. Three stable conformers of **1** were isolated and characterized, comprising a pair of enantiomers (**1**-(*P*, *P*, *P*, *P*) and **1**-(*M*, *M*, *M*, *M*)) and a mesomer (**1**-(*P*, *P*, *M*, *M*)). The increased flexibility of the helicene units resulted in broadening of the absorption and emission peaks for **1**, accompanied by an enhanced emission quantum yield. The chiral conformer of **1** exhibited a circular dichroic (CD) response extending up to a wavelength of 560 nm, which was extended further to 605 nm after protonation. In addition to that, a metallosupramolecular trimer (**3**) was prepared utilizing the chiral conformer of **1** as a building unit for coordination with (*cis*-dppp)Pd^{II}. This trimer exhibited a distinct CD response, indicating chiral transfer within the complex. These results offer compelling evidence of the potential of helical diazananographene as a responsive chiral optical chromophore and a versatile component for chiral metallosupramolecular assemblies.

Experimental Section

NMR spectra were acquired on a Bruker Spectrometers at 298 K in the solvents indicated. Chemical shifts are expressed in ppm units relative to TMS (0.00 ppm, 1H). Mass spectra were recorded using a Bruker time of flight mass spectrometer coupled with matrix-assisted laser desorption/ionization source (MALDI-TOF). Silica gel (300-400 mesh) was used for column chromatography. Ultraviolet/visible absorption spectra were recorded using Cary 5000 Spectrometer. Fluorescence spectra were acquired on a FLS-980 Fluorescence Spectrophotometer in the solvents indicated.

Funding Information

This work was supported by the National Natural Science Foundation of China (92061103, 21721001, 22101241).

Supporting Information

Experimental methods, detailed synthesis, additional data, ^{1}H and ^{13}C NMR spectra, mass spectra, additional optical spectra.

Conflict of Interest

The authors declare no competing financial interest.

References

(1) Bunz, U. H. F.; Engelhart, J. U.; Lindner, B. D.; Schaffroth, M. *Angew. Chem. Int. Ed.* **2013**, *52*, 3810.
(2) Liu, Z.; Fu, S.; Liu, X.; Narita, A.; Samorì, P.; Bonn, M.; Wang, H. I. *Adv. Sci.* **2022**, *9*, 2106055.
(3) Chen, Y.; Zhou, R.; Liu, X.; Yang, C.; Wang, T.; Shi, F.; Zhang, L. *Chem. Commun*. **2022**, *58*, 4671.
(4) Li, Y. L.; Zee, C.-T.; Lin, J. B.; Basile, V. M.; Muni, M.; Flores, M. D.; Munárriz, J.; Kaner, R. B.; Alexandrova, A. N.; Houk, K. N.; Tolbert, S. H.; Rubin, Y. *J. Am. Chem. Soc.* **2020**, *142*, 18093.
(5) Yao, X.; Zheng, W.; Osella, S.; Qiu, Z.; Fu, S.; Schollmeyer, D.; Müller, B.; Beljonne, D.; Bonn, M.; Wang, H. I.; Müllen, K.; Narita, A. *J. Am. Chem. Soc.* **2021**, *143*, 5654.
(6) Maiti, U. N.; Lee, W. J.; Lee, J. M.; Oh, Y.; Kim, J. Y.; Kim, J. E.; Shim, J.; Han, T. H.; Kim, S. O. *Adv. Mater*. **2014**, *26*, 40.
(7) Draper, S. M.; Gregg, D. J.; Madathil, R. *J. Am. Chem. Soc.* **2002**, *124*, 3486.

(8) Wang, X. Y.; Yao, X.; Narita, A.; Mullen, K. *Acc. Chem. Res.* **2019**, *52*, 2491.
(9) Castro-Fernández, S.; Cruz, C. M.; Mariz, I. F. A.; Márquez, I. R.; Jiménez, V. G.; Palomino Ruiz, L.; Cuerva, J. M.; Maçôas, E.; Campaña, A. G. *Angew. Chem. Int. Ed.* **2020**, *59*, 7139.
(10) Liu, Y.; Marszalek, T.; Müllen, K.; Pisula, W.; Feng, X. *Chem. Asian J.* **2016**, *11*, 2107.
(11) Martin, C. J.; Gil, B.; Perera, S. D.; Draper, S. M. *Chem. Commun.* **2011**, *47*, 3616.
(12) Chai, L.; Ju, Y. Y.; Xing, J. F.; Ma, X. H.; Zhao, X. J.; Tan, Y. Z. *Angew. Chem. Int. Ed.* **2022**, *134*, e202210268.
(13) Chai, L.; Li, J.-H.; Fang, H.-Z.; Xing, J.-F.; Ma, X.-H.; Zhao, X.-J.; Yang, Y.; Tan, Y.-Z. *J. Organomet. Chem.* **2023**, *1001*, 122877.
(14) Jin, E.; Yang, Q.; Ju, C.-W.; Chen, Q.; Landfester, K.; Bonn, M.; Müllen, K.; Liu, X.; Narita, A. *J. Am. Chem. Soc.* **2021**, *143*, 10403.
(15) Reger, D.; Schöll, K.; Hampel, F.; Maid, H.; Jux, N. *Chem. Eur. J.* **2021**, *27*, 1984.
(16) Wang, F.-F.; Wang, Y.-X.; Wu, Q.; Chai, L.; Chen, X.-W.; Tan, Y.-Z. *Angew. Chem. Int. Ed.* **2023**, *n/a*, e202315302.
(17) Cruz, C.; Castro-Fernández, S.; Maçôas, E.; Millán, A.; Campaña, A. *Synlett.* **2019**, *30*, 997.
(18) Kumar, V.; Bharathkumar, H. J.; Dongre, S. D.; Gonnade, R.; Krishnamoorthy, K.; Babu, S. S. *Angew. Chem. Int. Ed.* **2023**, *62*, e202311657.
(19) Xu, X.; Yang, Q.; Zhao, H.; Vasylevskyi, S.; Bonn, M.; Liu, X.; Narita, A. *Adv. Funct. Mater.* **2023**, *n/a*, 2308110.
(20) Rietsch, P.; Soyka, J.; Brülls, S.; Er, J.; Hoffmann, K.; Beerhues, J.; Sarkar, B.; Resch-Genger, U.; Eigler, S. *Chem. Commun.* **2019**, *55*, 10515.
(21) Li, S.; Li, R.; Zhang, Y.-K.; Wang, S.; Ma, B.; Zhang, B.; An, P. *Chem. Sci.* **2023**, *14*, 3286.
(22) Xu, X.; Xia, T.; Chen, X.-L.; Hao, X.; Liang, T.; Li, H.-R.; Gong, H.-Y. *New J. Chem.* **2022**, *46*, 11835.
(23) Gregg, D. J.; Bothe, E.; Höfer, P.; Passaniti, P.; Draper, S. M. *Inorg. Chem.* **2005**, *44*, 5654.
(24) Medel, M. A.; Hortigüela, L.; Lloveras, V.; Catalán-Toledo, J.; Miguel, D.; Mota, A. J.; Crivillers, N.; Campaña, A. G.; Morcillo, S. P. *ChemistryEurope* **2023**, *1*, e202300021.
(25) Ito, H.; Sakai, H.; Okayasu, Y.; Yuasa, J.; Mori, T.; Hasobe, T. *Chem. Eur. J.* **2018**, *24*, 16889.
(26) Graule, S.; Rudolph, M.; Vanthuyne, N.; Autschbach, J.; Roussel, C.; Crassous, J.; Réau, R., *J. Am. Chem. Soc.* **2009**, *131*, 3183.
(27) Takimoto, K.; Shimada, T.; Nagura, K.; Hill, J. P.; Nakanishi, T.; Yuge, H.; Ishihara, S.; Labuta, J.; Sato, H. *J. Am. Chem. Soc.* **2023**, *145*, 25160.
(28) Salerno, F.; Rice, B.; Schmidt, J. A.; Fuchter, M. J.; Nelson, J.; Jelfs, K. E. *Phys. Chem. Chem. Phys.* **2019,** *21*, 5059.
(29) Ikemoto, K.; Harada, S.; Yang, S.; Matsuno, T.; Isobe, H. *Angew. Chem. Int. Ed.* **2022**, *61*, e202114305.
(30) Xu, K.; Fu, Y.; Zhou, Y.; Hennersdorf, F.; Machata, P.; Vincon, I.; Weigand, J. J.; Popov, A. A.; Berger, R.; Feng, X. *Angew. Chem. Int. Ed.* **2017**, *56*, 15876.
(31) Schuster, N. J.; Hernández Sánchez, R.; Bukharina, D.; Kotov, N. A.; Berova, N.; Ng, F.; Steigerwald, M. L.; Nuckolls, C. *J. Am. Chem. Soc.* **2018**, *140*, 6235.
(32) Chen, F.; Tanaka, T.; Hong, Y. S.; Mori, T.; Kim, D.; Osuka, A. *Angew. Chem. Int. Ed.* **2017**, *56*, 14688.
(33) Guo, X.; Yuan, Z.; Zhu, Y.; Li, Z.; Huang, R.; Xia, Z.; Zhang, W.; Li, Y.; Wang, J. *Angew. Chem. Int. Ed.* **2019**, *58*, 16966.
(34) Liu, G.; Koch, T.; Li, Y.; Doltsinis, N. L.; Wang, Z. *Angew. Chem. Int. Ed.* **2019**, *58*, 178.
(35) Stephens, P. J.; Devlin, F. J.; Chabalowski, C. F.; Frisch, M. J. *J. Phys. Chem.* **1994**, *98*, 11623.
(36) Grimme, S.; Antony, J.; Ehrlich, S.; Krieg, H. *J. Chem. Phys.* **2010,** *132*, 254.
(37) Grimme, S.; Ehrlich, S.; Goerigk, L. *J. Comput. Chem.* **2011**, *32*, 1456.
(38) Ditchfield, R.; Hehre, W. J.; Pople, J. A. *J. Chem. Phys.* **2003**, *54*, 724.
(39) Ammon, F.; Sauer, S. T.; Lippert, R.; Lungerich, D.; Reger, D.; Hampel, F.; Jux, N. *Org. Chem. Front.* **2017**, *4*, 861.
(40) Martin, M. M.; Hampel, F.; Jux, N. *Chem. Eur. J.* **2020**, *26*, 10210.